

# Ultrasonic reflectivity technique for the characterization of fiber-matrix interface in metal matrix composites

Theodore E. Matikas

*US Air Force, Wright Laboratory, Materials Directorate, WL/MLLP, Wright-Patterson Air Force Base, Dayton, Ohio 45433-7817*

Prasanna Karpur

*Structural Integrity Division, Research Institute, University of Dayton, Dayton, Ohio 45469-0127*

(Received 22 December 1992; accepted for publication 2 March 1993)

An ultrasonic plane wave reflected by a cylindrical fiber embedded in a homogeneous isotropic matrix is modeled. The model calculates the "back-reflection" coefficient by taking into account the properties of the fiber and the matrix, the ultrasonic wavelength, the angle of incidence, and a coefficient called "shear stiffness coefficient" which characterizes the elastic behavior between the fiber and the matrix. Results obtained from the theoretical analysis for a model metal matrix composite system are shown. The theory developed in this paper and some of the results obtained are equally applicable in ceramic matrix fiber reinforced composites.

## I. INTRODUCTION

The properties of a composite system are dominated and determined by the behavior of the interface between the fiber and the matrix materials. It is at the interface that the load transfer takes place and the crack resistance exists. As a result, the characterization of the interfaces between various combinations of different types of fibers and matrix materials is of great interest to the researchers who are developing the composite materials. The objective of the evaluation of the interface would be to estimate the achieved interfacial elastic behavior between the fiber and the matrix. A common method of the material selection and interface analysis process is to first fabricate a model monofilament composite made up of a single fiber of interest embedded in the matrix material of choice. The sample is usually made by diffusion bonding two plates of the matrix material with a fiber of interest placed between them. The monofilament model composite is traditionally further subjected to some destructive tests to characterize the interface. Since the destructive tests render the sample unusable, there is a need to develop an ultrasonic nondestructive tool for the characterization of the interface in the model composite during the design and development of a new composite system. Although the ultrasonic technique will be developed for a monofilament composite, the method should be equally applicable to study the fiber-matrix interface in the outermost layers of a real, multifiber composite system.

An ultrasonic back-reflectivity technique has been developed to complement other existing techniques for the characterization of the interfacial behavior in fiber reinforced model composites. These techniques may be (1) destructive: fiber "pull-out" and "push-out" tests; the "fiber fragmentation" technique implemented by subjecting the model composite to axial loading to induce the fragmentation of the fiber and by measuring the size of the fragments which would be linked to the "interfacial load transfer behavior";<sup>1</sup> (2) nondestructive: ultrasonic imag-

ing of the fiber fragmentation,<sup>2-5</sup> in conjunction with advanced signal processing techniques.<sup>6</sup>

The ultrasonic characterization of the interface is achieved by the analysis of the back-reflected signal<sup>5</sup> from the fiber-matrix interface. The advantages of the ultrasonic back-reflectivity technique are several. One, the method is completely nondestructive and facilitates the use of the same sample for the tests (fatigue and creep) other than the interface analysis. Two, the technique can provide the distribution and variation of the interfacial properties along the length of the fiber thereby facilitating better process control. Three, the interface can be monitored for degradation and changes during fatigue tests for life prediction.

The goal of this study is to develop a theoretical model which will aid in the determination of various experimental parameters such as the frequency of ultrasound and angle of incidence while providing the vital relationship necessary to interpret the future experimental results. The theoretical model will consider the reflection of an ultrasonic wave front from a single fiber embedded in a homogeneous isotropic matrix.

## II. MODEL

Figure 1 shows the geometry of the problem: a plane wave  $\exp[i(\omega t + k_1 z_i)]$  is obliquely incident at an angle  $\theta$  on a model monofilament composite immersed in a fluid of mass density  $\rho_1$ , and in a plane normal to the axis of the fiber ( $\omega$  denotes the angular frequency and  $k_1$  is the wave number in the fluid).

For the development of the theoretical model, the composite is simulated by an infinitely extended plate consisting of an isotropic matrix with an embedded cylindrical isotropic and homogeneous fiber (which is justified at the wavelength of interest—frequency of ultrasonic waves:  $f < 50$  MHz). Further, since the ultrasonic beam is assumed to be incident on the composite such that the refracted wave is always normal to the fiber circumference (back-reflection interrogation technique), without the loss

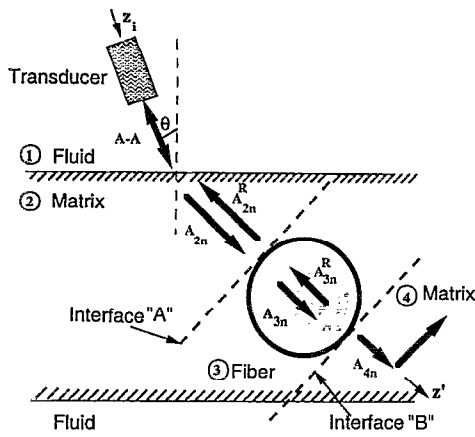


FIG. 1. Geometry of the problem.

of the generality, the cylindrical fiber of diameter  $d'$  can be replaced with an infinitely extended homogeneous isotropic layer of thickness equal to the diameter of the fiber (shown in dotted lines in Fig. 1). Although it is relatively easy to model the fiber as a cylinder<sup>7</sup> and use the Bessel function response of the cylinder, the present formulation of a plate will not deviate substantially from the reflected amplitude at the center of the main lobe of the Bessel function (the center of the main lobe of the Bessel function is the only point of interest for this study because the ultrasonic beam is normally incident to the circumference of the cylindrical fiber). Effects of attenuation and diffraction<sup>8</sup> can also be considered in the model if the matrix and the fiber thicknesses are significant. However, since the matrix is relatively thin (approximately five times the wavelength)<sup>8</sup> for this application, the effect of attenuation and diffraction are omitted here.

In the following analysis the symbol  $\theta_{2n}$  denotes the propagation angle of (longitudinal or shear) refracted waves in the matrix defined by the Snell's law:

$$\sin \theta_{2n} = \frac{c_{2n}}{c_1} \sin \theta,$$

where  $c_1$  is the velocity of propagation of ultrasonic waves in the fluid and  $c_{2n}$  is the longitudinal or shear velocity in the matrix, and the subscript  $n$  is  $L$  in the case of a longitudinal refracted wave, and "S" in the case of a shear refracted wave.

As the acoustic wave is incident on the composite, a part of the energy will be reflected into the fluid and another part of the energy will be transmitted to the matrix of mass density  $\rho_2$ . Two types of waves can be propagated in the matrix:

(i) In the case of a refracted longitudinal wave of displacement amplitude  $A_{2L}$ , the transmission coefficient is given by

$$T_L = \frac{2}{M} \cos 2\theta_{2S}. \quad (1)$$

(ii) In the case of a mode converted shear wave of displacement amplitude  $A_{2S}$ , the transmission coefficient is given by

$$T_S = -\frac{2}{M} \left( \frac{c_{2S}}{c_{2L}} \right)^2 \sin 2\theta_{2L}, \quad (2)$$

with the abbreviation

$$M = \left( \frac{c_{2S}}{c_{2L}} \right)^2 \sin 2\theta_{2L} \sin 2\theta_{2S} + \cos^2 2\theta_{2S} + \frac{\rho_1 c_1 \cos \theta_{2L}}{\rho_2 c_{2L} \cos \theta}. \quad (3)$$

Now consider an acoustic wave (either longitudinal or shear) of displacement amplitude  $A_{2n}$  propagating in the positive direction of the  $z'$  axis and normally incident on the matrix-fiber interface (Fig. 1). The fiber is denoted by medium 3 (mass density of the fiber:  $\rho_3$ , longitudinal or shear velocity of propagation of ultrasonic waves in the fiber:  $c_{3n}$ ), and the upper and lower regions of the matrix are denoted by medium 2 and medium 4, respectively. The two interfaces between the matrix and the plate representing the fiber are normal to the  $z'$  axis with the "upper" interface—interface  $A$ —located on the plane  $z' = d_n$  ( $d_n$  is the distance through which the refracted waves travel in the matrix before incidence on the fiber,  $d_L \neq d_S$  for a given  $\theta$  because of the assumption that the reflection coefficient is always measured when the refracted wave is normal to the circumference of the fiber) and the "lower" interface—interface  $B$ —on the plane  $z' = d_n + d'$ . In medium 2, for a given mode of wave propagation, two wave fronts are propagating: one incident ( $A_{2n}$ ) on the interface  $A$  and one reflected ( $A_{2n}^R$ ) from that interface. Also, in medium 3 two wave fronts are propagating: one incident ( $A_{3n}$ ) on the interface  $B$  and one reflected ( $A_{3n}^R$ ) from that interface. In medium 4, only one wave (the transmitted wave of amplitude  $A_{4n}$ ) is considered because of the configuration shown in Fig. 1 (i.e., no back reflection due to the angle of incidence at the lower interface between the matrix and the fluid). Therefore, medium 4 is equivalent to a semi-infinite medium.

The displacements and the related stresses (in the direction of  $z'$  axis) in the media 2, 3, and 4 are given by the expressions

$$\begin{aligned} u_{2n} &= A_{2n} \exp[i(\omega t + k_{2n} z')] + A_{2n}^R \exp[i(\omega t - k_{2n} z')], \\ u_{3n} &= A_{3n} \exp[i(\omega t + k_{3n} z')] + A_{3n}^R \exp[i(\omega t - k_{3n} z')], \\ u_{4n} &= A_{4n} \exp[i(\omega t + k_{2n} z')]; \end{aligned} \quad (4)$$

$$\begin{aligned} \sigma_{2n} &= Z_{2n} c_{2n} \frac{\partial u_{2n}}{\partial z'}, \\ \sigma_{3n} &= Z_{3n} c_{3n} \frac{\partial u_{3n}}{\partial z'}, \\ \sigma_{4n} &= Z_{2n} c_{2n} \frac{\partial u_{4n}}{\partial z'}, \end{aligned} \quad (5)$$

where  $k_{2n}$ ,  $k_{3n}$  are wave numbers and  $Z_{2n}$ ,  $Z_{3n}$  are acoustic impedances, and the numbers in the subscripts denote the medium with which the quantity is associated.

From Eq. (5) and by taking into account Eq. (4), the stresses in media 2, 3, and 4 can be expressed as

$$\begin{aligned}\sigma_{2n} &= iZ_{2n}c_{2n}k_{2n}\{A_{2n}\exp[i(\omega t + k_{2n}z')] \\ &\quad - A_{2n}^R\exp[i(\omega t - k_{2n}z')]\}, \\ \sigma_{3n} &= iZ_{3n}c_{3n}k_{3n}\{A_{3n}\exp[i(\omega t + k_{3n}z')] \\ &\quad - A_{3n}^R\exp[i(\omega t - k_{3n}z')]\}, \\ \sigma_{4n} &= iZ_{2n}c_{2n}k_{2n}\{A_{4n}\exp[i(\omega t + k_{2n}z')]\}.\end{aligned}\quad (6)$$

#### A. The interfacial conditions between the matrix and the fiber

The interface between the matrix and the fiber is modeled by (i) assuming continuity of normal displacements and conservation of normal and shear stresses at the interface, and (ii) by allowing the discontinuity of shear displacements at the interface. It is assumed that the vibration is transmitted instantaneously from one medium to the other by weightless springs with an equivalent rigidity of  $N_n$  (GPa/ $\mu\text{m}$ ).

The interfacial stiffness coefficient  $N_n$  of the matrix-fiber boundaries (upper and lower) can generally be different around the circumference, due to the fabrication conditions or due to the use of different material for each matrix plate. Thus, consider two different coefficients  $N_n$  and  $\tilde{N}_n$ , one for each interface. Accordingly, the interface conditions are

$$\begin{aligned}\{\sigma^P\} &= 0 \quad \{\sigma^T\} = 0 \quad [u^P] = 0, \\ \sigma^T &= N_n [u^T] \quad (\text{interface } A)\end{aligned}\quad (7)$$

or

$$\sigma^T = \tilde{N}_n [u^T] \quad (\text{interface } B),$$

where the superscripts  $P$  and  $T$  denote normal or tangential displacements ( $u$ ) and stresses ( $\sigma$ ) respectively; the square brackets denote the jump of a function across the interface, and the curly brackets denote the vectorial resultant of stresses at the interface. The linearity of Eq. (7) is based on the assumption of small amplitudes of vibrations, which is justified for ultrasonic applications wherein the amplitudes of displacements are around a few angstroms. Also,

$$\begin{aligned}u^P &= \mathbf{u} \quad \sigma^P = \sigma_{ij}m_j, \\ u^T &= \mathbf{u} - u^P \mathbf{m} \quad \sigma^T = \sigma - \sigma^P \mathbf{m},\end{aligned}\quad (8)$$

where  $\mathbf{m}$  is the outward unit normal to medium 3 and  $\mathbf{u}$  and  $\sigma$  denote the displacement and traction vectors at the interface.

At the two interfaces  $A$  and  $B$ , the displacement jumps are given by

$$\begin{aligned}[u^T]_{z'=d_n} &= u_{3n}(d_n, t) - u_{2n}(d_n, t), \\ [u^T]_{z'=d_n+d'} &= u_{4n}(d_n+d', t) - u_{3n}(d_n+d', t),\end{aligned}\quad (9)$$

and the stresses at the boundaries due to the spring forces are defined by

$$\sigma^T = N_n [u_{3n}(d_n, t) - u_{2n}(d_n, t)], \quad (10)$$

$$\sigma^{\tilde{T}} = \tilde{N}_n [u_{4n}(d_n+d', t) - u_{3n}(d_n+d', t)].$$

With the assumption of instantaneously transmitted stresses through the springs from medium 2 to medium 3 and from 3 to 4 (i.e., negligible inertial forces), the boundary conditions are

(i) at the interface  $A$

$$\sigma_{2n}(d_n, t) = \sigma_{3n}(d_n, t) = \sigma^T(t); \quad (11)$$

(ii) at the interface  $B$

$$\sigma_{3n}(d_n+d', t) = \sigma_{4n}(d_n+d', t) = \sigma^{\tilde{T}}(t), \quad (12)$$

and the pressure reflection coefficient  $W_n = A_{2n}^R/A_{2n}$  can be derived from Eqs. (4), (6), (11), and (12):

$$W_n = \frac{Q1_n - Q2_n}{Q3_n - Q4_n} e_n, \quad (13)$$

where  $Q1_n$ ,  $Q2_n$ ,  $Q3_n$ , and  $Q4_n$  are complex quantities expressed by the equations

$$\begin{aligned}Q1_n &= X_n^2 Y_n^2 (e'_n - 1) + N_n \tilde{N}_n (X_n^2 - Y_n^2) (1 - e'_n), \\ Q2_n &= X_n Y_n \{ \tilde{N}_n [X_n (1 + e'_n) + Y_n (1 - e'_n)] \\ &\quad + N_n [X_n (1 + e''_n) - Y_n (1 - e''_n)] \}, \\ Q3_n &= X_n^2 Y_n^2 (e'_n - 1) + N_n \tilde{N}_n [(X_n^2 + Y_n^2) (1 - e'_n) \\ &\quad + 2X_n Y_n (1 + e'_n)],\end{aligned}\quad (14)$$

$$\begin{aligned}Q4_n &= X_n Y_n \{ \tilde{N}_n [X_n (1 + e'_n) + Y_n (1 - e'_n)] \\ &\quad + N_n [X_n (1 + e'_n) + Y_n (1 - e'_n)] \},\end{aligned}$$

with

$$\begin{aligned}X_n &= Z_{2n}c_{2n}k_{2n} = 2\pi\rho_2c_{2n}f, \\ Y_n &= Z_{3n}c_{3n}k_{3n} = 2\pi\rho_3c_{3n}f, \\ e'_n &= \exp[ik_{3n}2d'], \\ e_n &= \exp[ik_{2n}2d_n], \\ d_n &= \frac{1}{2} \left( \frac{\tilde{d}}{\cos 2\theta_{2n}} - d' \right),\end{aligned}\quad (15)$$

and  $\tilde{d}$  denotes the thickness of the sample. Note that the case of infinitely rigid springs ( $N_n, \tilde{N}_n \rightarrow \infty$ ) corresponds to perfect continuity of displacements across the interface (implies a mere contact for longitudinal waves and infinitely rigid interfaces for shear waves; see the appendix for details), and the coefficient  $W_n$  is given by the simplified expression

$$W_n = \frac{(X_n^2 - Y_n^2)(1 - e')}{(X_n^2 + Y_n^2)(1 - e') + 2X_n Y_n (1 + e')}, \quad (16)$$

whereas the case of infinitely compliant springs ( $N_n, \tilde{N}_n = 0$ ) corresponds to complete discontinuity of displacements (noncontacting surfaces for longitudinal waves and both noncontacting and merely contacting surfaces—assuming no residual stresses at the interface—for shear

waves; see appendix for details). Hence, in the case of complete discontinuity of displacement, the boundary of the matrix becomes a free surface and no energy is transmitted into the fiber. As a result, the magnitude of the reflection coefficient (13) becomes

$$|W_n| = 1 \quad (\text{even if } \tilde{N}_n \rightarrow \infty), \quad (17)$$

representing total reflection from the fiber.

Finally, consider an ultrasonic wave of amplitude  $A_{2n}^R$  to be incident on the interface between media 2 and 1. The longitudinal and shear transmission coefficients at this interface can be obtained by

$$TF_L = \frac{2}{M} \frac{\rho_1 c_1 \cos \theta_{2L} \cos 2\theta_{2S}}{\rho_2 c_{2L} \cos \theta}, \quad (18)$$

$$TF_S = \frac{2}{M} \frac{\rho_1 c_1 \cos \theta_{2L} \sin 2\theta_{2S}}{\rho_2 c_{2L} \cos \theta}. \quad (19)$$

The back reflection from the fiber, represented by  $A-A$  in Fig. 1, is the wave front of interest for this study.

The back-reflection coefficients for longitudinal (20) and shear (21) interrogation respectively,

$$R_L = T_L W_L TF_L, \quad (20)$$

$$R_S = T_S W_S TF_S, \quad (21)$$

are dependent on the following:

- (a) the properties of the matrix (density  $\rho_2$ , longitudinal  $c_{2L}$ , and shear  $c_{2S}$  velocities),
- (b) the properties of the fiber (density  $\rho_3$ , longitudinal  $c_{3L}$ , and shear  $c_{3S}$  velocities),
- (c) the diameter of the fiber ( $d'$ ),
- (d) the angle of incidence ( $\theta$ ),
- (e) the frequency ( $f$ ) of interrogation, and
- (f) the interfacial stiffness coefficients ( $N_n, \tilde{N}_n$ ).

The stiffness coefficient is dependent on the wave type because of the different mechanism of stress transfer for compressional or shear displacement waves as discussed in the following sections.

## B. Longitudinal wave back-reflection coefficient

In this case, the direction of oscillation of the material particles is normal to the fiber surface. As a result, a mere contact can transmit the displacement and the normal stresses across the interface. Hence, this type of wave is not sensitive to various bonding conditions. As a result, the stiffness coefficient  $N_n$  can take only two values:  $N_L=0$  (for longitudinal waves, complete unbond which implies physical separation of the matrix and the fiber with no contact) or  $\infty$  (for longitudinal waves, this implies all possibilities from a mere contact to a completely rigid bond).

## C. Shear wave back-reflection coefficient

In this case, a mode converted shear wave propagating in the matrix will be incident normally to the fiber. Therefore, the direction of oscillation of the material particles will be tangential to the fiber surface. As a result, the interface is exposed to shear stresses which are sensitive to

the interfacial bonding. Hence, in the case of a mere contact, no part of the tangential displacement will be transferred to the fiber from the matrix at the interface. On the other hand, when the matrix and the fiber are bonded at the interface, a part of the tangential displacement will be transferred to the fiber from the matrix. The magnitude of the transferred displacement will be proportional to the rigidity of bonding. As a result, there will be a tangential "elastic" relative displacement at the interface which is proportional to the shear traction, and is characterized by the newly proposed positive coefficient  $N_S$ . The underlying assumptions and modeling in the derivation of Eq. (21) for the back-reflection coefficient of the shear waves allow for intermediate bonding between  $N_S=0$  and  $N_S=\infty$  representing different degrees of chemical/mechanical bonding. The existence of such a "degree of chemical/mechanical bonding" has been shown in the literature.<sup>2-5</sup>

The shear stress behavior of the interfaces is also affected by the existence of residual stresses due to the mismatch of the coefficient of thermal expansion.<sup>3,5,9</sup> The compressive radial component of the residual stresses at the interface<sup>9</sup> facilitates the transfer of shear stresses across the interface at room temperature even in the absence of chemical bonding thereby providing a lower limit to the experimentally measured interfacial shear stiffness coefficient  $N_{Smin}$ . However, for this study, the existence of the residual stresses is ignored. The methodology for the estimation of the residual stresses and the related necessary modifications of the experimentally measured shear stiffness coefficient (effective stiffness coefficient) can be found in the literature.<sup>2,5,10</sup> The properties and the reactivity of the two materials in contact provide an upper limit to the interface stiffness coefficient  $N_{Smax}$ . Again, since the residual stresses are ignored for this theoretical modeling,  $N_{Smax}$  will be taken to be completely due to the interface. However, the achieved interfacial shear stiffness coefficient  $N_S$  will be generally between  $N_{Smin}$  and  $N_{Smax}$  depending on the processing parameters and conditions such as temperature, pressure, surface preparation, etc.

## III. NUMERICAL RESULTS—DISCUSSION

The longitudinal waves are insensitive to the interfacial conditions as discussed above. Hence, all the results and discussions in the remaining part of this paper will be for the shear wave interrogation of the interface.

The back-reflection coefficient amplitude as a function of interfacial stiffness and frequency for a Ti-6Al-4V/SCS-6 composite (fiber diameter of 152  $\mu\text{m}$ ) is shown in Fig. 2(a). In the range of frequencies of 10–50 MHz two resonance peaks occur, one at 15 MHz and the other at 40 MHz. In between the two resonances, a dip is also evident. Fig. 2(b) [isolevel contour map representation of Fig. 2(a)] shows that the frequency at which the dip occurs, for a given stiffness coefficient, shifts up followed by a downshift as the stiffness increases from 0 (complete unbond) to 20 GPa/ $\mu\text{m}$  (almost a rigid bond). This shift is analogous to a behavior that would be produced by an apparent non-linear variation in the effective diameter of the fiber. Additional discussions of this behavior are provided in a later

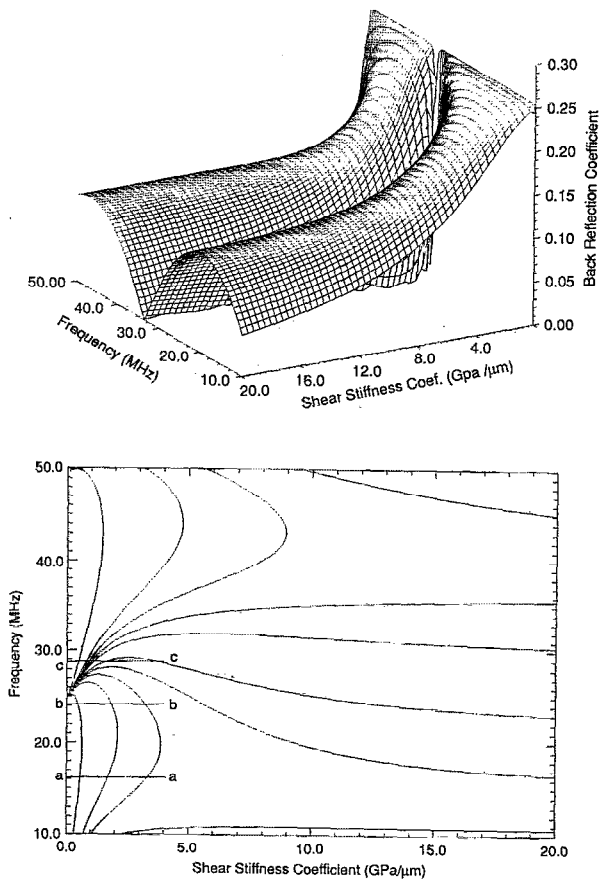


FIG. 2. (a) Back-reflection coefficient amplitude as a function of interfacial shear stiffness coefficient and frequency. (b) Isolevel contour map representation of the Data in (a).

section of this paper and also can be found in the literature.<sup>2,3</sup> Figures 2(a) and 2(b) also aid in the selection of an appropriate frequency for the experimental evaluation<sup>10</sup> of the matrix-fiber interfacial properties.

An appropriate ultrasonic frequency for the experimental interrogation is an important parameter necessary to improve the sensitivity of the technique. An estimation of the appropriate frequency of interrogation can be obtained from Figs. 3(a), 3(b), and 3(c) which are derived from Figs. 2(a) and 2(b). The curves shown in Figs. 3(a), 3(b), and 3(c) are cross sections of the back-reflection coefficient surface [shown in Fig. 2(b) by lines *a-a*, *b-b*, and *c-c*, respectively] for frequencies of 16, 24, and 29 MHz. If a near resonance frequency such as 16 MHz [Fig. 3(a)] is selected for the experiments, the reflection coefficient changes from 0.252 for a complete disbond to 0.105 for a completely rigid interface 7.6 dB). However, if the frequency of interrogation is such as 24 MHz [Fig. 3(b)], the range of the reflection coefficient is 0.252–0.026 (19.7 dB). The increase in the sensitivity in Fig. 3(b) compared to that of Fig. 3(a) is obtained because the frequency of interrogation in Fig. 3(b) is close to a resonance dip thereby exploiting the slope of the surface as it approaches the resonance dip. It is imperative that the frequency of interrogation should only approach the resonance dip from below because, otherwise, the reflection coefficient behav-

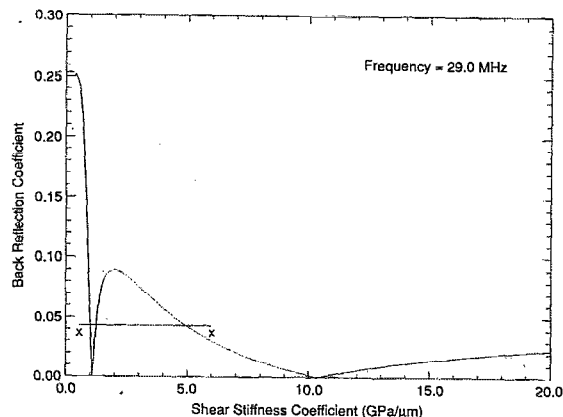
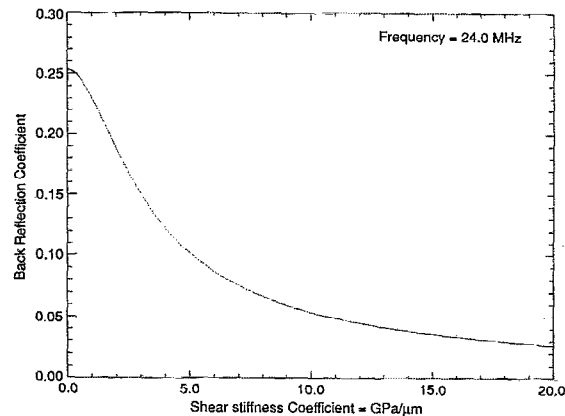
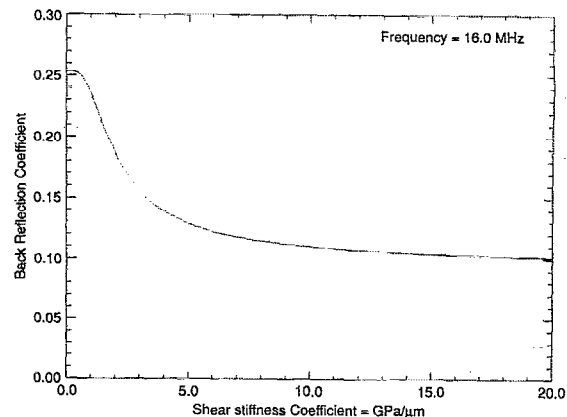


FIG. 3. (a) Back-reflection coefficient amplitude vs shear stiffness coefficient for a frequency near a resonance peak (16.0 MHz). (b) Back-reflection coefficient amplitude vs shear stiffness coefficient for a frequency slightly lower than the resonance dip (24.0 MHz). (c) Back-reflection coefficient amplitude vs shear stiffness coefficient for a frequency slightly higher than the resonance dip (29.0 MHz).

ior at 29 MHz [Fig. 3(c)] is not monotonic with respect to the interfacial stiffness coefficient, the same back reflected amplitude may correspond to various interfacial stiffness [as in line *x-x* in Fig. 3(c)].

A further understanding of the behavior of the reflection coefficient as a function of the frequency of interrogation and the interfacial stiffness coefficient can be obtained by generating the back-reflection coefficient surface for a wider range of frequencies (1–150 MHz). Figure 4(a) shows the surface of the back-reflection coefficient and Fig.

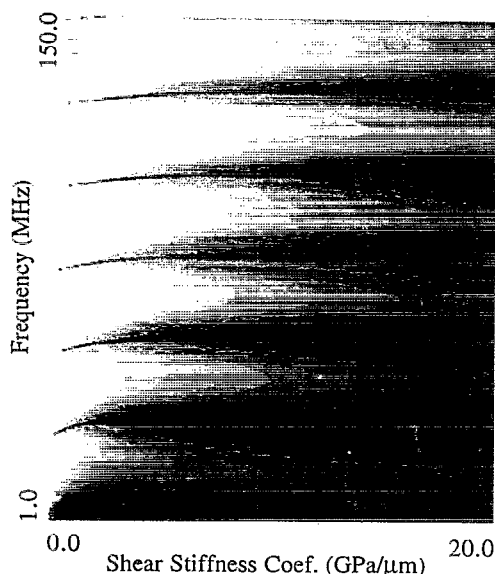
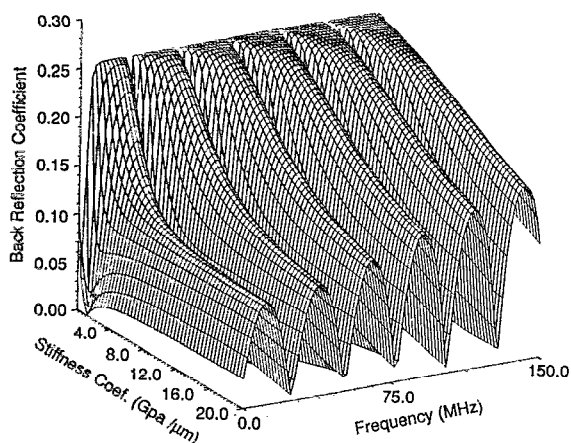


FIG. 4. (a) Back-reflection coefficient amplitude as a function of interfacial shear stiffness and for a range of frequencies 1–150 MHz. (b) Isopleth projection of the data in (a).

4(b) shows the corresponding isopleth projection. Figures 5(a)–5(c) are cross sections of the surface at three different interfacial stiffness coefficients [Fig. 5(a) at almost a disbond of 2.0 GPa/μm, Fig. 5(b) at an intermediate level of bonding of 10.0 GPa/μm, and Fig. 5(c) with a completely rigid interfacial bonding of 100.0 GPa/μm]. Figures 6(a)–(c) are derived by taking cross sections of the surface at three different resonant peak frequencies, 15, 66, 141 MHz, respectively.

Figures 4(a) and 4(b) demonstrate the overall nonlinear behavior of the reflection coefficient as a function of the frequency and stiffness coefficient. The isopleth representation shown in Fig. 4(b) clearly indicates the contour of the resonance dips evident in Fig. 4(a). From Fig. 4(b) it is evident that the resonant dips run parallel to each other at higher stiffness coefficients. However, at lower ranges of the stiffness coefficient, the nonlinear shift of the resonance dips [such as discussed earlier for Figs. 2(a) and 2(b)] shows a decreased sensitivity to the stiffness coefficient as the frequency of interrogation increases. This decreased sensitivity is evidenced due to the fact that the resonance

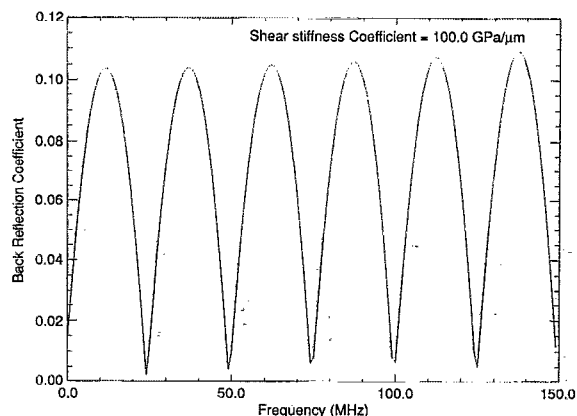
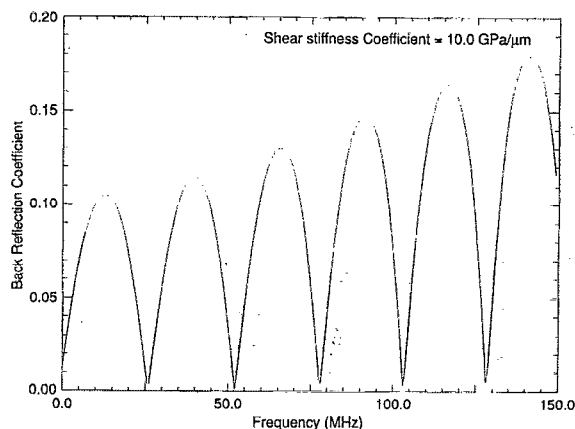
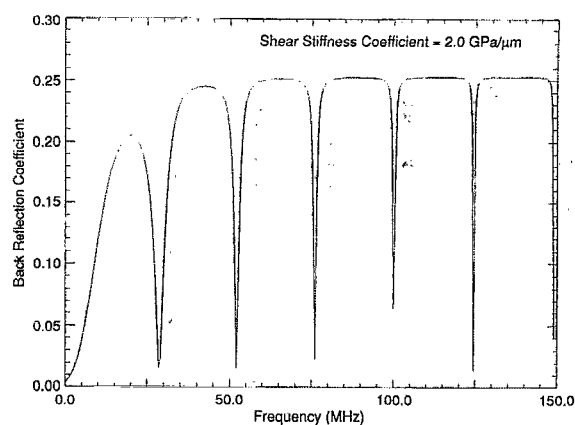


FIG. 5. (a) Back-reflection coefficient amplitude vs frequency for a flexible bond between the matrix and the fiber (shear stiffness coefficient: 2.0 GPa/μm). (b) Back-reflection coefficient amplitude vs frequency for an intermediate condition of bonding between the matrix and the fiber (shear stiffness coefficient: 10.0 GPa/μm). (c) Back-reflection coefficient amplitude vs frequency for “infinitely” rigid bond between the matrix and the fiber (shear stiffness coefficient: 100.0 GPa/μm).

dips at progressively higher frequencies show progressively less nonlinearity.

Figures 5(a)–5(c) show the response of the interfaces with different stiffness coefficients when excited with different frequencies. When the bond has an almost infinite stiffness coefficient (for all practical purposes, 100 GPa/μm), the resonance curves [Fig. 5(c)] obtained are the well-known symmetric lobes with the resonance peaks of the same amplitudes. However, as the stiffness coefficient

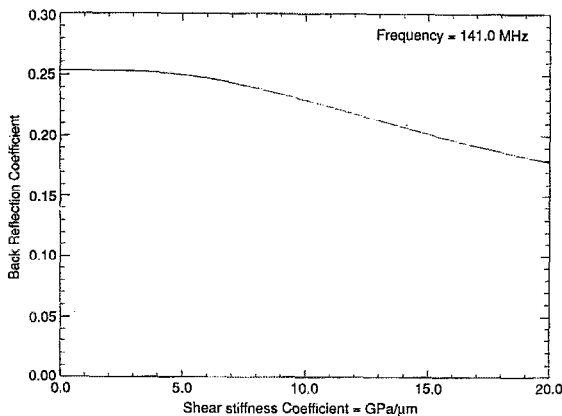
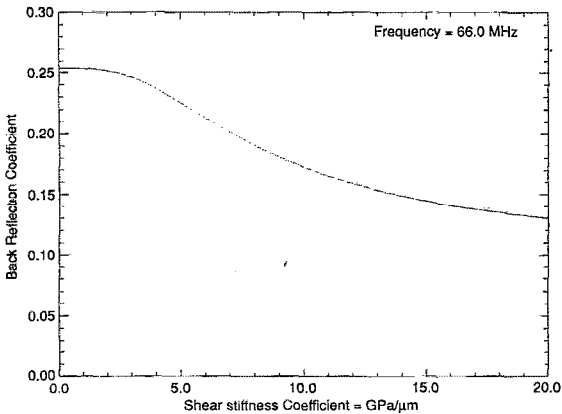
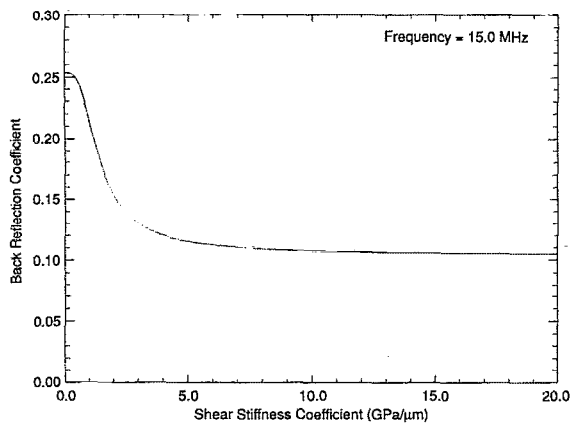


FIG. 6. Resonant back-reflection coefficient amplitude vs shear stiffness coefficient for a given frequency of (a) 15.0 MHz, (b) 66.0 MHz, (c) 141.0 MHz.

of the bond progressively decreases, the obtained resonance lobes become progressively nonsymmetric as shown in Figs. 5(a) and 5(b) wherein the amplitudes of resonance peaks are higher and higher as the frequency increases.

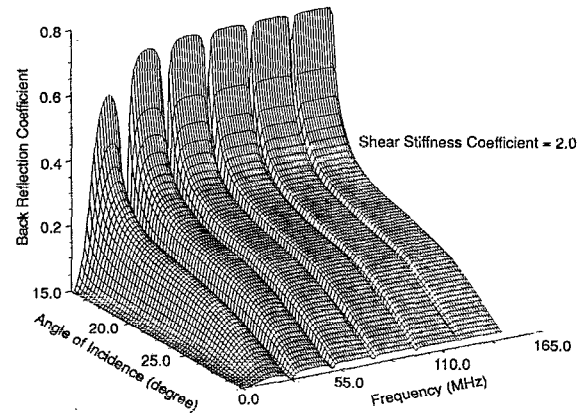
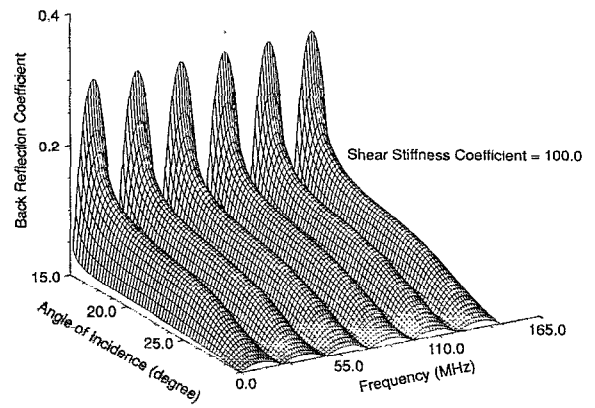


FIG. 7. (a) Back-reflection coefficient amplitude as a function of frequency and angle of incidence in the case of an “infinitely” rigid bond (shear stiffness coefficient: 100.0 GPa/μm). (b) Back-reflection coefficient amplitude as a function of frequency and angle of incidence in the case of a flexible bond (shear stiffness coefficient: 2.0 GPa/μm).

Figures 6(a)–6(c) provide a revealing insight into the behavior of the interface when interrogated with different frequencies. It is apparent from these figures that the range of change in the back-reflected amplitude due to the changes in the interfacial bonding is enhanced at lower frequencies than that at higher frequencies. This implies that longer wavelengths are effective to evaluate the interfacial bonding because of their sensitivity to the changes in the stiffness of a relatively flexible bond [as indicated by the slope of the curve in Fig. 6(a)]. Conversely, shorter wavelengths are ineffective to evaluate the interfacial stiffness due to their inability to sense small changes in the stiffness coefficient of a relatively flexible bond [as indicated by the slope of the curve in Fig. 6(c)]. Similar results have been reported by Jones and Whittier,<sup>11</sup> wherein they used dis-

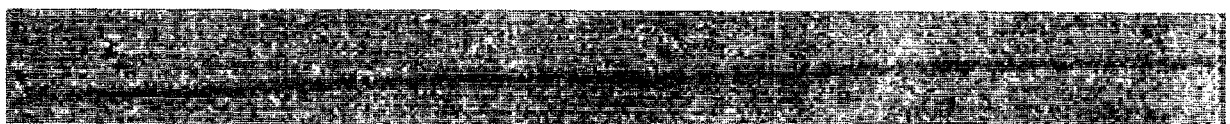


FIG. 8. Ultrasonic image of a single SCS-6 fiber embedded in Ti-6Al-4V matrix using a 50-MHz transducer at normal incidence—longitudinal wave interrogation.

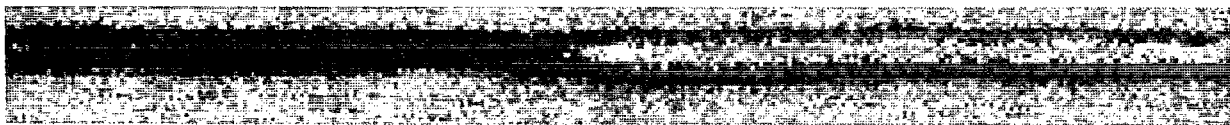


FIG. 9. Ultrasonic image of a single SCS-6 fiber embedded in Ti-6Al-4V matrix using a 25-MHz transducer at oblique incidence (between the first and the second critical angle), shear wave interrogation.

person determinant analysis to evaluate adhesive joints between two solid half-spaces.

Figures 7(a) and 7(b) show the dependence of the back-reflection coefficient on the frequency and the angle of incidence for a given stiffness coefficient. Figure 7(a) is obtained for an infinitely rigid bond (in this instance, 100 GPa/ $\mu\text{m}$  of stiffness coefficient) and shows symmetric resonance peaks for all angles of incidence. However, in Fig. 7(b), for a flexible bond (in this instance 2.0 GPa/ $\mu\text{m}$  of stiffness coefficient), the resonance peak amplitudes are strongly dependent on the angle of incidence (increasing resonance amplitude with frequency). Further, the resonance peaks show a plateau at higher frequencies compared to the smooth, rounded resonance lobes with a unique maximum amplitude at lower frequencies. Also, while the resonance dips (defined by the ratio of the diameter of the fiber and the wavelength) remain equally spaced, the corners of the plateau progressively become sharper with the increase in the incident frequency. This means that higher frequencies begin to see this flexible bond as equivalent to a disbond implying that shorter wavelengths are less sensitive to the changes in stiffness coefficient of the bonding. Although the asymmetric behavior is enhanced at lower angles of incidence, it is evident at all angles of incidence. The important implication of the Figs. 7(a) and 7(b) is that, when the interface is rigid, swept frequency experiments at different angles of incidence will produce the symmetric profile as shown in Fig. 7(a). However, if the interface is flexible, the swept frequency experiment will produce the behavior as shown in Fig. 7(b).

#### IV. CONCLUSION

A theoretical model has been developed for the characterization of fiber/matrix "interfacial stiffness" in composites using shear wave back-reflection coefficient interrogation. The model has been used to define the optimum experimental parameters such as frequency of interrogation and angle of incidence. The results show the need for selecting the frequency of interrogation carefully to avoid ambiguities wherein the ultrasonic reflection coefficient will not have a monotonic relationship to the shear stiffness coefficient. Also, a suitable selection of the frequency based on the newly developed theoretical modeling will provide a better dynamic range and sensitivity to the reflection coefficient analysis. Such an increase in the sensitivity can be obtained by avoiding the resonance peaks and valleys of the reflectivity surface.

Another important conclusion obtained from the reflectivity analysis is that higher frequencies ( $> 25$  MHz for titanium-based alloy matrix) of shear wave interrogation are not capable of detecting flexible bonds. On the other hand, lower frequencies ( $< 25$  MHz) are relatively more sensitive to flexible bonds ( $\lesssim 20$  GPa/ $\mu\text{m}$ ), but insensitive to small changes in stiffness if the bond is already rigid ( $\gtrsim 20$  GPa/ $\mu\text{m}$ ). A swept frequency reflectivity analysis at various angles of incidence can be used effectively to evaluate the interface because of the existence of plateaux at higher frequencies when the bonding is flexible ( $\lesssim 20$  GPa/ $\mu\text{m}$ ). The sensitivity of shear waves has been experimentally demonstrated by the C-scan images provided in the Appendix.

#### ACKNOWLEDGMENTS

This work was supported by and performed on site in the Materials Directorate, Wright Laboratory, Wright-Patterson Air Force Base, Ohio 45433-7817, Contract No. F33615-89-C-5612 (P. Karpur). Theodore E. Matikas is a National Research Council Associate.

#### APPENDIX

In order to compare longitudinal and shear interrogation and show the advantage of the use of shear waves for the evaluation of various interface conditions a single SiC-6 fiber embedded in Ti-6Al-4V matrix was imaged using (1) a 50-MHz focused ultrasonic transducer at normal incidence, and (2) a 25-MHz focused ultrasonic transducer at oblique incidence (between the first and the second critical angle). The incident wave, longitudinal in case (1) and shear in case (2), was scanned on the fiber to produce the C-scan images A1 and A2. The results in Figs. 8 and 9 show that the shear waves compared to longitudinal waves of approximately the same wavelength are more sensitive to the various interfacial conditions.

- <sup>1</sup>A. Kelly and W. R. Tyson, *J. Mech. Phys. Solids* **13**, 329 (1965).
- <sup>2</sup>P. Karpur, T. E. Matikas, S. Krishnamurthy, and N. Ashbaugh, in *19th Annual Review in Progress in Quantitative Nondestructive Evaluation*, Vol. 11, edited by D. O. Thompson and D. E. Chimenti (Plenum, New York, 1993).
- <sup>3</sup>P. Karpur, T. E. Matikas, and S. Krishnamurthy, *Proceedings of the 7th Technical Conference on Composite Materials*, edited by the American Society of Composites, 1992, p. 420 (1992).
- <sup>4</sup>P. Karpur, T. E. Matikas, and S. Krishnamurthy, "Ultrasound as a Tool for the Characterization of the Matrix-Fiber Interface in Metal Matrix Composites", presented in the *Mechanics of Composites Review*, 1992 (unpublished).
- <sup>5</sup>T. E. Matikas and P. Karpur, in *19th Annual Review in Progress in Quantitative Nondestructive Evaluation*, Vol. 11, edited by D. O.

Thompson and D. E. Chimenti (Plenum, New York, 1993).

<sup>6</sup>L. E. Mann, T. E. Matikas, P. Karpur, and S. Krishnamurthy, Proc. 1992 IEEE Ultrasonics Symp. **1**, 355 (1992).

<sup>7</sup>T. E. Matikas and P. Karpur, "Back-Reflection of Ultrasonic Shear Waves from Homogeneous Cylindrical Fibers Embedded in Metallic Matrix" (unpublished).

<sup>8</sup>T. E. Matikas and P. Karpur, "Effects of Attenuation and Diffraction on the Ultrasonic Back-Reflection Technique for the Interface Characterization of Metal Matrix Composites" (unpublished).

<sup>9</sup>D. Coker, N. E. Ashbaugh, and T. Nicholas, presented in the ASTM Symposium on Thermomechanical Fatigue Behavior of Materials, STP 1186, (1991) (in press).

<sup>10</sup>P. Karpur, T. E. Matikas, and S. Krishnamurthy, "Characterization of the Fiber-Matrix Interphase/Interface for Mechanics of Continuous Fiber Reinforced Metal Matrix and Ceramic Matrix Composites," 1993 (to be published in the Journal of Composites Science and Technology).

<sup>11</sup>J. P. Jones, and J. S. Whittier, J. Appl. Mechan., p. 905 (1967).